arXiv:1406.4795v1 [cond-mat.mtrl-sci] 18 Jun 2014

Spin-helical Dirac states in graphene induced by polar-substrate surfaces with giant spin-orbit interaction: a new platform for spintronics

S. V. Eremeev,[1,2,3] I. A. Nechaev,[2,3] P. M. Echenique,[3,4,5] and E. V. Chulkov[3,4,5]

[1]*Institute of Strength Physics and Materials Science, 634021, Tomsk, Russia*
[2]*Tomsk State University, 634050, Tomsk, Russia*
[3]*Donostia International Physics Center (DIPC), 20018 San Sebastián/Donostia, Basque Country, Spain*
[4]*Departamento de Física de Materiales UPV/EHU, Facultad de Ciencias Químicas, UPV/EHU, Apdo. 1072, 20080 Sebastián/Donostia, Basque Country, Spain*
[5]*Centro de Física de Materiales CFM - MPC, Centro Mixto CSIC-UPV/EHU, 20080 San Sebastián/Donostia, Basque Country, Spain*

(Dated: February 29, 2024)

Spintronics, or spin electronics, is aimed at efficient control and manipulation of spin degrees of freedom in electron systems. To comply with demands of nowaday spintronics, the studies of electron systems hosting giant spin-orbit-split electron states have become one of the most important directions providing us with a basis for desirable spintronics devices. In construction of such devices, it is also tempting to involve graphene, which has attracted great attention because of its unique and remarkable electronic properties and was recognized as a viable replacement for silicon in electronics. In this case, a challenging goal is to make graphene Dirac states spin-polarized. Here, we report on absolutely new promising pathway to create spin-polarized Dirac states based on coupling of graphene and polar-substrate surface states with giant Rashba-type spin-splitting. We demonstrate how the spin-helical Dirac states are formed in graphene deposited on the surface of BiTeCl. This coupling induces spin separation of the originally spin-degenerate graphene states and results in fully helical in-plane spin polarization of the Dirac electrons.

PACS numbers: 73.20.-r, 79.60.-i

INTRODUCTION

Graphene is a fascinating material, which has attracted great attention because of its unique electronic properties [1, 2]. In graphene spintronics, many efforts were made to realize a robust control of electron spins by, e.g., magnetoelectric coupling or spin-orbit interaction (SOI) [3–5]. Main hopes were pinned on the SOI effect, which can be directly observed [6, 7].

Some interesting phenomena, such as quantum spin Hall effect [8], quantum anomalous Hall effect [9], and other phenomena were predicted in graphene. However, the intrinsic spin-orbit splitting in pristine graphene is proved to be too weak to produce an observable effect and to realize practical applications [8, 10, 11]. The major challenge in graphene spintronics is to make graphene Dirac states spin-polarized. In principle, it can be realized by applying an extrinsic SOI, i.e., by placing the grapnene in a proper medium with a strong spin-orbit coupling. Numerous previous works, both experimental and theoretical, have been aimed at enhancement of graphene SOI via adatoms deposition [9, 12–14] or growth of graphene on metal substrates [15–19].

In the present paper, we propose a new pathway to manipulate the electronic and spin properties of graphene by its depositing on a polar-substrate surface possessing a giant Rashba-type spin-split surface state. We state that one of the efficient mechanisms responsible for appearance of spin-polarised Dirac states in graphene is the coupling of two two-dimensional (2D) electron systems: Dirac electrons of graphene and Rashba electrons of the mentioned surface state. To corroborate our statement, we have chosen the most suitable 2D Rashba-electron system formed by electons in the surface state at the Te-terminated surface of bismuth tellurohalides. Here, on the base of relativistic density functional theory (DFT) calculations, we show that graphene deposited on BiTeCl is the system with unique electronic properties, in which the strong hybridization of Dirac and Rashba electrons gives rise to spin-helical Dirac states.

METHOD

Our calculations were based on DFT as implemented in the Vienna *ab initio* simulation package VASP, [28, 29]. The generalized gradient approximation (GGA) of Perdew, Burke, and Ernzerhof (PBE) [30] to the exchange correlation (XC) potential has been implemented. The interaction between the ion cores and valence electrons was described by the projector augmented-wave method [31, 32]. The Hamiltonian contained the scalar relativistic corrections, and the spin-orbit coupling was taken into account by the second variation method [33]. To simulate BiTeCl substrate we consider a 24 atomic layer slab. Hydrogen monolayer was used to passivate

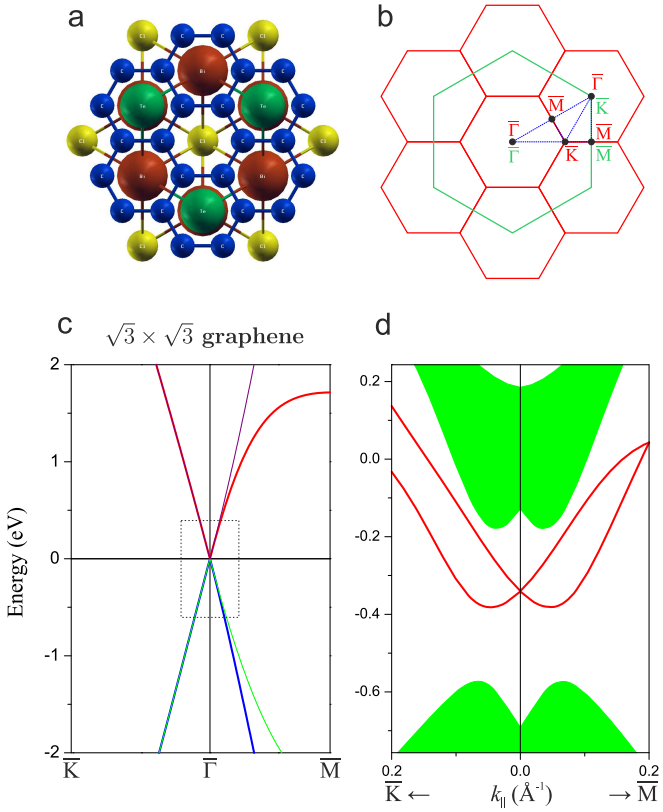


FIG. 1: (Color online) **Atomic structure of graphene on BiTeCl and electronic spectra of the pristine graphene and Te-terminated BiTeCl surface.** (**a**) Top view for the $\sqrt{3}\times\sqrt{3}$ graphene on the Te-terminated surface of BiTeCl. Carbon atoms are shown by dark blue balls; green, maroon, and yellow balls denote first-layer Te atom, second-layer Bi atom, and third-layer Cl atom, respectively; (**b**) Scheme of $\sqrt{3}\times\sqrt{3}$ folding of the 2D BZ of graphene: green and red colors correspond to the 1×1 and $\sqrt{3}\times\sqrt{3}$ BZs, respectively; (**c**) Band structure of the $\sqrt{3}\times\sqrt{3}$ graphene; (**d**) Electronic spectrum of the Te-terminated BiTeCl surface. The Rashba-split surface state is shown by red line, projected bulk band structure is depicted by green areas.

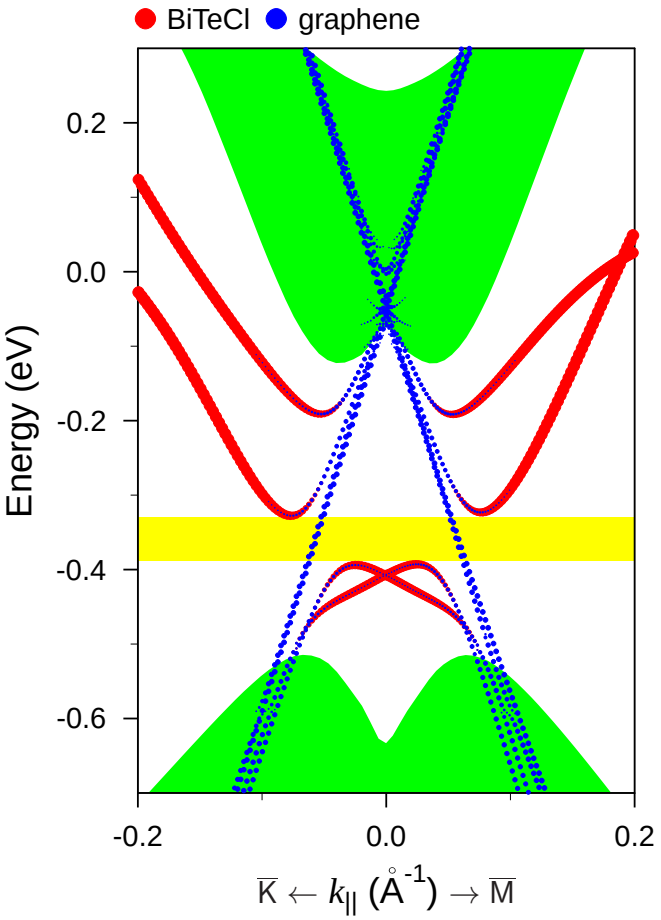


FIG. 2: (Color online) **Electronic structure of graphene@BiTeCl.** Band structure of BiTeCl(0001) slab with $\sqrt{3}\times\sqrt{3}$ graphene on Te-terminated surface. Red and blue circles denotes weights of the states localized in the outermost three layers (1-st TL) of BiTeCl and in graphene layer, respectively. Shaded by green color regions indicate projected bulk bands of substrate.

the chlorine side of the slab as was described in Ref. [20]. The positions of atoms in the graphene layer and within three outermost atomic layers of the BiTeCl slab were optimized including SOI self-consistently. The distance between the substrate and the graphene layer was found to be of ≈ 3.35Å. The atoms of the deeper layers were kept fixed at the bulk crystalline positions. The k-point mesh of $9\times9\times1$ was used for the Brillouin zone of the surface unit cell.

RESULTS

Recently, it was shown that the Te-terminated surface of non-centrosymmetric hexagonal-structured polar-semiconductor compounds BiTe(Cl,Br,I) meet requirements for spintronics applications, since these systems hold a giant Rashba spin splitting of a free-electron-like surface state at the $\bar{\Gamma}$ point [20–25]. The mentioned bismuth tellurohalides are characterized by ionic bonding with large charge transfer from bismuth to halide- and tellutium-atomic layers. The spin-split surface states at the Te-terminated surface emerge by splitting off from the lowest conduction band, owing to the decreasing potential within the near-surface layers [20], which is a consequence of strong ionicity. One can expect that deposition of graphene on BiTe(Cl,Br,I), can result in a strong interaction and hybridization of the Rashba and Dirac 2D electrons. In designing such systems, it is important to match the lattice parameters of the contacting materials. The in-plane hexagonal parameter of BiTeCl matches perfectly with the parameter of $\sqrt{3}\times\sqrt{3}$ graphene. Thus, the deposited graphene should not undergo the in-plane strain [Fig. 1(a)]. In the $\sqrt{3}\times\sqrt{3}$

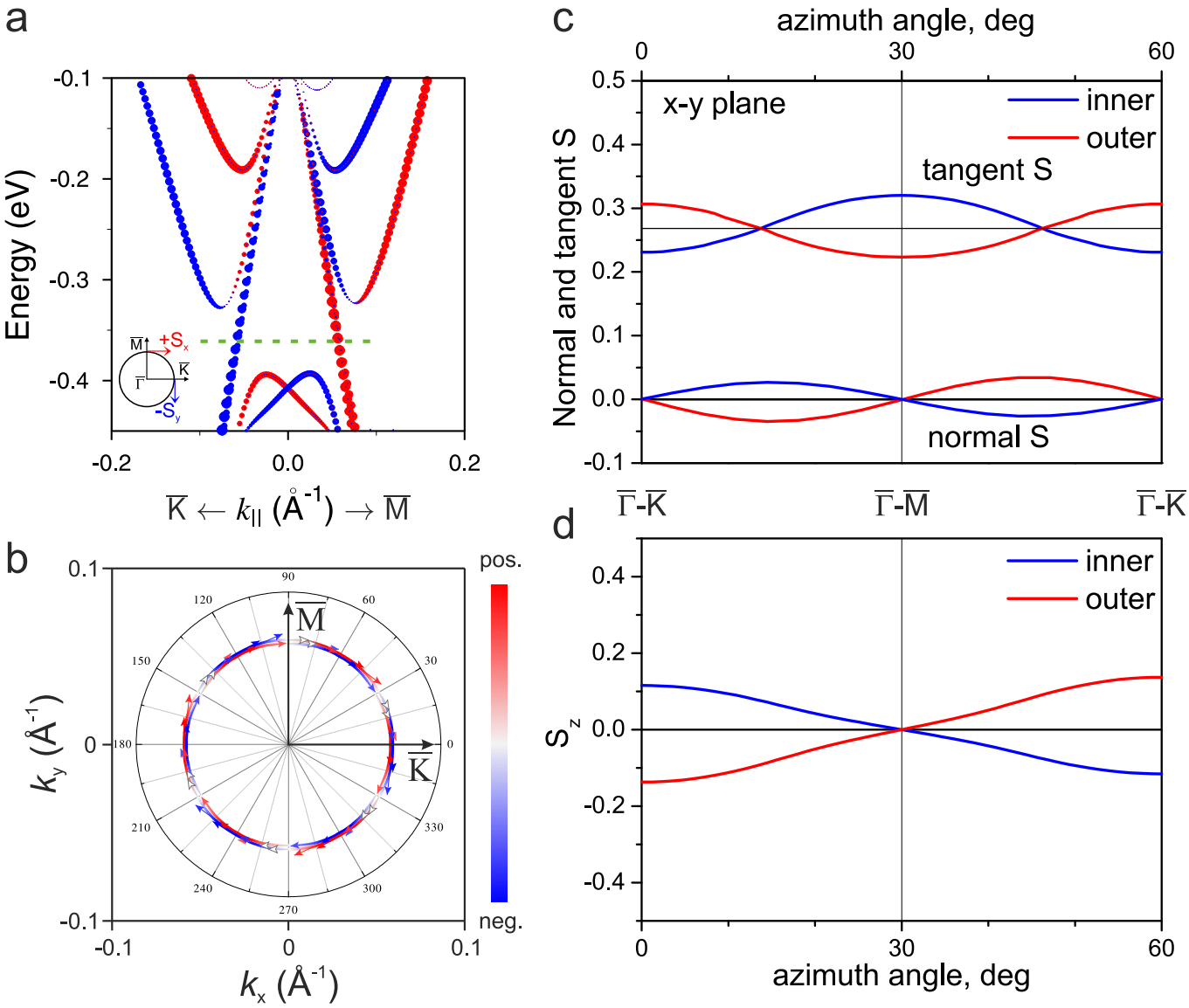


FIG. 3: (Color online) **Spin structure of the surface states.** (**a**) The spin-resolved electronic spectrum of the surface states where the filled circles represent the weight of the states multiplied by the value of the in-plane spin component (red and blue colors denote positive and negative values of spin, respectively, for mutually perpendicular $\bar{\Gamma}-\bar{\mathrm{M}}$ and $\bar{\Gamma}-\bar{\mathrm{K}}$ directions as schematically shown in inset); (**b**) Constant energy contours for graphene Dirac-cone bands at energy of -365 meV, marked by dashed green line in panel (a). Arrows adjacent to the contours denote the in-plane spin component. The out-of-plane spin component is indicated by the colour with red and blue corresponding to the upward and downward directions, respectively. White colour arrows indicate fully in-plane spin alignment; Azimuthal dependencies of the graphene spin components, including the in-plane components in the tangent and normal directions to the contours (**c**) and out-of-plane component (**d**), inner and outer Dirac contours shown by blue and red, respectively.

structure, the Brillouin zone of graphene takes a third of the original one [Fig. 1(b)]. Under this folding, the $\bar{\mathrm{K}}$-point Dirac cone of graphene appears as four-fold degenerate $\bar{\Gamma}$ state [Fig. 1(c)] with linear dispersion in the vicinity of the Dirac point (Fig. 1(c), the dotted-line rectangle). Thus, both the Dirac state and the Rashba state of the pristine substrate [Fig. 1(d)] reside in the Brillouin zone center.

The interaction of the two 2D electron systems results in a strong modification of the spectra with respect to the constituents (Fig. 2). In the upper part of the gap, at large $k_{\|}$ the Rashba states of BiTeCl are preserved, while at $k_{\|} \lesssim 0.1$ Å^{-1} both inner and outer branches of the Rashba states rapidly become strongly hybridized with graphene cone states, and already at $k_{\|} \approx 0.05$ Å^{-1} they are completely localized within the graphene layer, dispersing towards the Dirac point, which is immersed in the conduction band of the substrate bulk states. In

the lower part of the gap, two of four graphene bands are hybridized with the substrate forming hole-like Rashba state near the valence band, which is completely localized within substrate layers in the vicinity of the $\bar{\Gamma}$ point. Thus, hybridization of two graphene branches with the Rashba state of the BiTeCl substrate leads to a break of both branches of the Rashba states at small $k_\parallel$ in such a way that its degeneracy point appears near the valence band or, to the contrary, the Rashba states break two graphene branches. Other two Dirac branches remain unchanged and localized in the graphene layer for all $k_\parallel$. As a result of these changes, in the middle part of the bulk band gap within the energy interval of 70 meV (see yellow stripe in Fig. 2) two almost degenerate Dirac states of graphene survive. The small SOI-induced $k_\parallel$-splitting for the Dirac cones is less then 0.002 Å^{-1}.

The spin structure of the surface states within the $\bar{\Gamma}$ band gap is shown in Fig. 3(a). As seen in the figure, at large $k_\parallel$ the Rashba branches preserve the spin polarization of the clean Te-terminated BiTeCl surface: they demonstrate counter-clockwise and clockwise in-plane helicity for the inner and outer branches, respectively. At $k_\parallel < 0.1$ Å^{-1}, where due to hybridization the Rashba branches turn into the Dirac states and start to be localized at the graphene layer, the spin helicity of the graphene band hybridizing with the outer branch becomes the same as that of the inner branch. Consequently, both hybridized graphene bands have the counter-clockwise spin polarization. It certainly would mean that two remaining non-hybridized Dirac bands should be characterized by the clockwise spin polarization, as it is confirmed by the spin-resolved bands presented in Fig. 3(a). Thus, and this is the main issue of the present study, the hybridization between the graphene and substrate-Rashba-split 2D electrons provides the helical spin separation of the graphene Dirac states.

As was mentioned above, the most interesting feature of the graphene@BiTeCl spectrum is the energy window of 70 meV width, where the Dirac states of graphene exist only (see yellow stripe in Fig. 2). The two almost degenerate Dirac states have the same in-plane spin polarization, which can be clearly seen in Fig. 3(b), where spin-resolved constant energy contours in the middle of this energy window are shown. Both Dirac states, apart from the in-plane clockwise spin polarization, also demonstrate the presence of the out-of-plane spin component, which is intrinsic feature of the spin-polarized states at hexagonal surfaces. The detailed spin texture is illustrated in Figs. 3(c) and (d). Fig. 3(c) shows the azimuthal dependencies of the in-plane spin components in the tangent and normal directions to the inner and outer Dirac contours. One can see that the tangent component for both bands demonstrates variation around the value of 0.27, while the normal component experiences small variations near zero spin value. For both bands, the out-of-plane spin component S_z [Fig. 3(d)] also varies near zero but the variations are significantly larger than those for the normal component. Nevertheless, the maximal out-of-plane spin values, which are observed along the $\bar{\Gamma} - \bar{\mathrm{K}}$ directions, are three times smaller than the magnitude of the tangent in-plane spin component. Furthermore, the signs of both normal and out-of-plane spin components are opposite for the inner and outer almost degenerate Dirac contours, what results in a fully helical net in-plane spin polarization of the Dirac electrons.

DISCUSSION

Apparently, the revealed possibility to create the helical spin-polarized Dirac electrons in graphene opens up new horizons in the graphene-based spintronics. The mentioned spin texture of the graphene Dirac states is important to come out as a consequence of the strong hybridization between graphene and giant Rashba-split states of the Te-terminated surface of the polar substrate BiTeCl. Due to excellent matching lattice parameters of BiTeCl and graphene, the graphene@BiTeCl system can be easily realized on practice. The reported energy interval of ~ 70 meV in the middle part of the projected bulk energy gap, where the spin-polarized Dirac states solely exist, is sufficiently enough for spintronics applications. However, it should be noted that this energy interval can be wider in a real system, since the band gap is normally underestimated within the DFT. As shown both by experiment [24] and by the *GW* bulk calculations [26], the bulk band gap in BiTeCl is a factor of two larger than that predicted by the DFT. In order to actively bring the spin-polarized Dirac states located in the middle part of the gap into play, the chemical potential of the system should be decreased by ~ 350 meV with respect to the Fermi level obtained in the present calculation. The chemical potential tuning can be realized by applying electric field or doping hole-donating adsorbates. The latter approach seems to be preferable. As was recently shown for Au/Si system, supporting Rashba-split surface state, the Fermi level position can be effectively tuned within the range of ~ 350 meV by choosing appropriate adsorbate species [27].

Except the spin-polarized Dirac states in the middle part of the gap, the surface states in upper and lower parts of the bulk gap may also be of considerable interest, because in the respective energy regions the helical Dirac states of graphene and Rashba spin-split states coexists. Various intriguing physical phenomena related to decay of elementary excitations in the states with different velocities can be expected.

We believe that our findings will stimulate further theoretical and experimental investigations of spin-polarized Dirac fermions which is a key matter for prospective spintronics applications.

ACKNOWLEDGEMENTS

We acknowledge partial support from the Basque Country Government, Departamento de Educación, Universidades e Investigación (Grant No. IT-756-13), the Spanish Ministerio de Ciencia e Innovación (Grant No. FIS2010-19609-C02-01), and the Ministry of Education and Science of Russian Federation (Grant No. 2.8575.2013).

[1] A. K. Geim, K. S. Novoselov, Nat. Mater **6**, 183 (2007).
[2] A. H. Castro Neto, F. Guinea, N. M. R. Peres, K. S. Novoselov, A. K. Geim, Rev. Mod. Phys. **81**, 109 (2009).
[3] I. Žutić, J. Fabian, S. Das Sarma, Rev. Mod. Phys. **76**, 323 (2004).
[4] D. D. Awschalom, M. E. Flatte, Nat. Phys **3**, 153 (2007).
[5] Z. Zhang, C. Chen, W. Guo, Phys. Rev. Lett. **103**, 187204 (2009).
[6] Y. K. Kato, R. C. Myers, A. C. Gossard, D. D. Awschalom, Science **306**, 1910 (2004).
[7] J. Wunderlich, B. Kaestner, J. Sinova, T. Jungwirth, Phys. Rev. Lett. **94**, 047204 (2005).
[8] C. L. Kane, E. J. Mele, Phys. Rev. Lett. **95**, 226801 (2005).
[9] Z. Qiao, S. A. Yang, W. Feng, W.-K. Tse, J. Ding, Y. Yao, et al., Phys. Rev. B **82**, 161414 (2010).
[10] Y. Yao, F. Ye, X.-L. Qi, S.-C. Zhang, Z. Fang, Phys. Rev. B **75**, 041401 (2007).
[11] M. Gmitra, S. Konschuh, C. Ertler, C. Ambrosch-Draxl, J. Fabian, Phys. Rev. B **80**, 235431 (2009).
[12] A. H. Castro Neto and F. Guinea, Phys. Rev. Lett. **103**, 026804 (2009).
[13] S. Abdelouahed, A. Ernst, J. Henk, I.V. Maznichenko, and I. Mertig, Phys. Rev. B **82**, 125424 (2010).
[14] C. Weeks, J. Hu, J. Alicea, M. Franz, and R. Wu, Phys. Rev. X **1**, 021001 (2011).
[15] Yu. S. Dedkov, M. Fonin, U. Rüdiger, and C. Laubschat, Phys. Rev. Lett. **100**, 107602 (2008).
[16] A. Varykhalov, J. Saánchez-Barriga, A. M. Shikin, C. Biswas, E. Vescovo, A. Rybkin, D. Marchenko, and O. Rader, Phys. Rev. Lett. **101**, 157601 (2008).
[17] W. A. de Heer, C. Berger, X. Wu, M. Sprinkle, Y. Hu, M. Ruan, J. A. Stroscio, Ph. N. First, R. Haddon, B. Piot, C. Faugeras, M. Potemski, and J.-S. Moon, J. Phys. D: Appl. Phys. **43**, 374007 (2010).
[18] Z. Y. Li, Z. Q. Yang, S. Qiao, J. Hu, R. Q. Wu, J. Phys.: Condens. Matter **23**, 225502 (2011).
[19] D. Marchenko, A. Varykhalov, M. R. Scholz, G. Bihlmayer, E. I. Rashba, A. Rybkin, A. M. Shikin, and O. Rader, Nature Commun. **6**, 1232 (2012).
[20] S. V. Eremeev, I. A. Nechaev, Yu. M. Koroteev, P. M. Echenique, and E. V. Chulkov, Phys. Rev. Lett. **108**, 246802 (2012).
[21] A. Crepaldi, L. Moreschini, G. Auteè, C. Tournier-Colletta, S. Moser, N. Virk, H. Berger, Ph. Bugnon, Y. J. Chang, K. Kern, A. Bostwick, E. Rotenberg, O. V. Yazyev, and M. Grioni, Phys. Rev. Lett. **109**, 096803 (2012).
[22] G. Landolt, S. V. Eremeev, Y. M. Koroteev, B. Slomski, S. Muff, T. Neupert, M. Kobayashi, V. N. Strocov, T. Schmitt, Z. S. Aliev, M. B. Babanly, I. R. Amiraslanov, E. V. Chulkov, J. Osterwalder, and J. H. Dil, Phys. Rev. Lett. **109**, 116403 (2012).
[23] S. V. Eremeev, A. I. Nechaev, E. V. Chulkov, JETP Lett. **96**, 437 (2012).
[24] M. Sakano, M. S. Bahramy, A. Katayama, T. Shimojima, H. Murakawa, Y. Kaneko, W. Malaeb, S. Shin, K. Ono, H. Kumigashira, R. Arita, N. Nagaosa, H. Y. Hwang, Y. Tokura, and K. Ishizaka, Phys. Rev. Lett. **110**, 107204 (2013).
[25] S. V. Eremeev, I. P. Rusinov, A. I. Nechaev, E. V. Chulkov, New J. Phys. **15**, 075015 (2013).
[26] I. P. Rusinov, I. A. Nechaev, S. V. Eremeev, C. Friedrich, S. Blügel, and E. V. Chulkov, Phys. Rev. B **87**, 205103 (2013).
[27] L. V. Bondarenko, D. V. Gruznev, A. A. Yakovlev, A. Y. Tupchaya, D. Usachov, O. Vilkov, A. Fedorov, D. V. Vyalikh, S. V. Eremeev, E. V. Chulkov, A. V. Zotov, and A. A. Saranin, Scientific Reports **3**, 1826 (2013).
[28] G. Kresse, J. Hafner, Phys. Rev. B **48**, 13115 (1993).
[29] G. Kresse, J. Furthmüller, Comput. Mater. Sci. **6**, 15 (1996).
[30] J.P. Perdew, K. Burke, and M. Ernzerhof, Phys. Rev. Lett. **77**, 3865 (1996); J.P. Perdew, K. Burke, and M. Ernzerhof, Phys. Rev. Lett. **78**, 1396(E) (1997).
[31] P.E. Blöchl, Phys. Rev. B **50**, 17953 (1994).
[32] G. Kresse, D. Joubert, Phys. Rev. B **59**, 1758 (1999).
[33] D.D. Koelling, B.N. Harmon, J. Phys. C **10**, 3107 (1977).